**Atmospheric
Chemistry
and Physics**

Exploring the atmospheric chemistry of nitrous acid (HONO) at a rural site in Southern China

X. Li[1,2], T. Brauers[2], R. Häseler[2], B. Bohn[2], H. Fuchs[2], A. Hofzumahaus[2], F. Holland[2], S. Lou[2,3,*], K. D. Lu[1,2], F. Rohrer[2], M. Hu[1], L. M. Zeng[1], Y. H. Zhang[1], R. M. Garland[4,**], H. Su[1,4], A. Nowak[5,***], A. Wiedensohler[5], N. Takegawa[6], M. Shao[1], and A. Wahner[2]

[1]College of Environmental Sciences and Engineering, Peking University, Beijing, China
[2]Institute for Energy and Climate Research, IEK-8, Research Center Jülich, Jülich, Germany
[3]School of Environmental Science and Technology, Shanghai Jiaotong University, Shanghai, China
[4]Max Planck Institute for Chemistry, Biogeochemistry Department, Mainz, Germany
[5]Leibniz Institute for Tropospheric Research, Leipzig, Germany
[6]Research Center for Advanced Science and Technology, University of Tokyo, Tokyo, Japan
[*]now at: Shanghai Academy of Environmental Sciences, Shanghai, China
[**]now at: Natural Resources and the Environment, CSIR, Pretoria, South Africa
[***]now at: Physikalisch Technische Bundesanstalt, Braunschweig, Germany

Correspondence to: T. Brauers (th.brauers@fz-juelich.de)

Abstract. We performed measurements of nitrous acid (HONO) during the PRIDE-PRD2006 campaign in the Pearl River Delta region 60 km north of Guangzhou, China, for 4 weeks in June 2006. HONO was measured by a LOPAP in-situ instrument which was setup in one of the campaign supersites along with a variety of instruments measuring hydroxyl radicals, trace gases, aerosols, and meteorological parameters. Maximum diurnal HONO mixing ratios of 1–5 ppb were observed during the nights. We found that the nighttime build-up of HONO can be attributed to the heterogeneous NO_2 to HONO conversion on ground surfaces and the $OH + NO$ reaction. In addition to elevated nighttime mixing ratios, measured noontime values of ≈ 200 ppt indicate the existence of a daytime source higher than the $OH + NO \rightarrow HONO$ reaction. Using the simultaneously recorded OH, NO, and HONO photolysis frequency, a daytime additional source strength of HONO (P_M) was calculated to be 0.77 ppb h^{-1} on average. This value compares well to previous measurements in other environments. Our analysis of P_M provides evidence that the photolysis of HNO_3 adsorbed on ground surfaces contributes to the HONO formation.

1 Introduction

Nitrous acid (HONO) is an important trace gas in the atmosphere due to its contribution to the cycles of nitrogen oxides (NO_x) and hydrogen oxides (HO_x) (Finlayson-Pitts and Pitts, 2000). The photolysis of HONO in the near ultraviolet spectral region (320 nm$<\lambda<$400 nm):

$$HONO + h\nu \rightarrow OH + NO \tag{R1}$$

provides a daytime source of hydroxyl radicals (OH) and nitrogen oxides (NO) independently from ozone photolysis and NO_2 concentrations. This feature is even more important after HONO accumulates under dark or low light conditions.

Observations of HONO in the troposphere were performed at many locations over the last 30 yr. These measurements revealed concentrations from several ppts in remote and clean areas (e.g. Zhou et al., 2002, 2007; Beine et al., 2006; Ren et al., 2010) up to several ppbs in more polluted environments (e.g. Febo et al., 1996; Stutz et al., 2002; Kanaya et al., 2007; Su et al., 2008a; Yu et al., 2009). Due to photolysis, HONO exhibits a diurnal variation with minima during the day. The highest reported values occurred during nighttime in heavily polluted megacities like Santiago, Chile (Elshorbany et al., 2009), and Guangzhou, China (Qin et al., 2009). The level
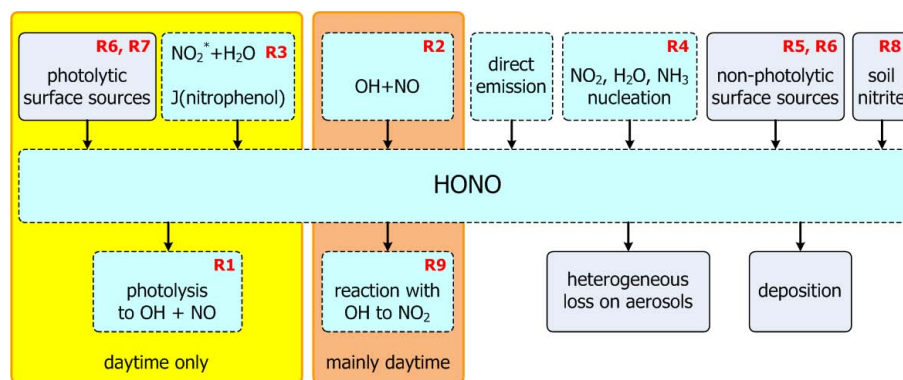
Fig. 1. Diagram of HONO budget in the troposphere. Boxes in light blue refers to gas phase reactions, while grey boxes refer to processes with various surfaces involved. Reactions in the yellow frame need solar radiation and thus only take place in daytime. When significant amount of OH radicals and NO exist, reactions in the light orange frame will also happen in night.

of HONO is related to the NO_x levels during all of these field experiments, however this relation is highly variable as indicated by the HONO to NO_x ratios determined in the above experiments, ranging from way below 1 % to well above 10 %.

Despite the importance of HONO in atmospheric chemistry, the HONO budget in the troposphere is not well understood since both emissions, homogeneous and heterogeneous processes influence the gas phase concentration of HONO. Figure 1 depicts the different pathways of HONO formation and loss. Direct emissions of HONO have been accessed through tunnel experiments and car exhaust analysis; the emission ratios of $HONO/NO_x$ are found to be 0.3–0.8 % (Kurtenbach et al., 2001, and references therein). These values are generally much lower than that from the field observations, indicating that the atmospheric HONO is mostly secondarily formed.

The reverse reaction of Reaction (R1) is the most important homogeneous reaction forming HONO.

$$OH + NO \xrightarrow{M} HONO \qquad (R2)$$

This reaction plays a role mainly during daytime when OH and NO are high (e.g. Alicke et al., 2003). However, in regions with significant amount of nighttime OH, e.g., Pearl River Delta in China (Lu et al., 2011), the contribution of Reaction (R2) to the nocturnal HONO formation might not be neglected. Li et al. (2008) found that the homogeneous reaction of photolytically excited NO_2 with H_2O can form OH and HONO.

$$NO_2 + h\nu(\lambda > 420\,nm) \rightarrow NO_2^*$$

$$NO_2^* + H_2O \rightarrow OH + HONO \qquad (R3)$$
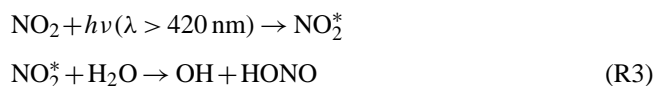
But its reaction rate and yield are still under discussion (Carr et al., 2009) and this mechanism does not significantly contributes to the atmospheric HONO formation (Sörgel et al., 2011a; Wong et al., 2011; Amedro et al., 2011). Laboratory

studies found that the photolysis of *ortho*-nitrophenols also leads to homogeneous HONO formation (Bejan et al., 2006). Although the estimated HONO formation rate of 100 ppt h^{-1} for 1 ppb nitrophenols at overhead sun could be a significant fraction of the total HONO formation rate during daytime, the relevance of this mechanism needs to be validated through field measurements. Based on theoretical calculations, Zhang and Tao (2010) proposed a gas phase HONO formation pathway through the homogeneous nucleation of NO_2, H_2O and NH_3.

$$2NO_2(g) + H_2O(g) + NH_3(g) \rightarrow HONO(g) + NH_4NO_3(s) \qquad (R4)$$
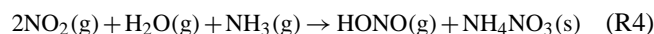
However, this reaction has not yet been tested by laboratory studies nor observed in field experiments.

Compared to the homogeneous HONO formation, heterogeneous formation of HONO on various surfaces is thought to be the most likely explanation of the observed high HONO concentrations. Laboratory studies revealed that NO_2 can be converted to HONO on wet surfaces.

$$NO_2 + NO_2 + H_2O_{ads} \xrightarrow{surf} HONO + HNO_3 \qquad (R5)$$

However, the source strength of Reaction (R5) is not exactly known and depends on various parameters including the gas phase NO_2 concentration, the surface water content, and the surface area density (Finlayson-Pitts et al., 2003). Laboratory studies also found a heterogeneous reduction of NO_2 forming HONO on soot particles or surfaces containing organic substrates (Ammann et al., 1998, 2005; Kleffmann et al., 1999; Bröske et al., 2003; Aubin and Abbatt, 2007). The proposed mechanism of this redox HONO formation is

$$NO_2 + HC_{red} \xrightarrow{surf} HONO + HC_{ox} \qquad (R6)$$

Reaction (R6) can be relevant for HONO formation under conditions of high NO_2 and soot loadings, i.e. in plumes (Kleffmann et al., 1999). Following Akimoto et al. (1987) who reported that Reaction (R6) was photo-enhanced, a photosensitized NO_2 reduction on organic surfaces has been observed

recently in many studies as an effective pathway producing HONO (George et al., 2005; Stemmler et al., 2006). The production rate of HONO is a complex function of the actinic flux, the surface area density and gas phase NO_2 concentration (Stemmler et al., 2007). At low NO_2, the HONO production is linearly increasing with NO_2; whilst the increase levels off when the NO_2 concentration reaches a certain point. The same phenomenon is also found for the actinic flux. The rate of the photosensitized reaction was 1–2 orders of magnitude more efficient than the dark reaction (George et al., 2005).

Both laboratory studies and field observations found that HONO can also be heterogeneously formed through the photolysis of adsorbed nitric acid (HNO_3) and nitrate (NO_3^-) at UV wavelengths (Zhou et al., 2002, 2003):

$$HNO_3/NO_3^- + h\nu \rightarrow HONO/NO_2^- + O \qquad (R7)$$

It is still an open question why the HNO_3-to-HONO conversion frequency necessary to explain the observed HONO production is orders of magnitude higher than the photolysis of HNO_3 in the gas and liquid phase (Zhou et al., 2003; Rohrer et al., 2005). However, a new field study by Zhou et al. (2011) provided evidence for a daytime source of nitrous acid caused by the photolysis of nitric acid on forest canopies.

Recently, Su et al. (2011) illustrated that the soil nitrite, which is formed through the biological nitrification and denitrification processes, can be a prominent HONO source. The HONO formation is via the following reversible acid-base reaction and partitioning between air and the aqueous phase of humid soil:

$$NO_2^-(aq) + H^+(aq) \leftrightarrow HNO_2(aq) \leftrightarrow HONO(g) \qquad (R8)$$
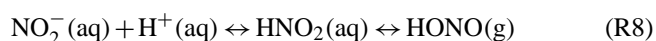
Its HONO production rate depends on the nitrite concentration, the pH value, the water content and the temperature of the soil. Values from 2 to 5 ppb h^{-1} were estimated for the field measurements in Xinken in Southern China, which can explain most HONO productions besides Reaction (R2) during daytime.

Compared to HONO formation, the loss processes of HONO are well understood. Besides Reaction (R1), HONO can be removed by reaction with OH.

$$HONO + OH \rightarrow H_2O + NO_2 \qquad (R9)$$
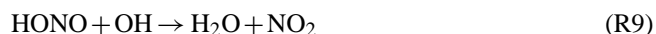
Reactions (R1) and (R9) are well established and they determine the HONO lifetime during daytime. Under typical daytime conditions the HONO lifetime is in the order of 20 min. Other gas phase reactions of HONO, e.g. self reaction or reaction with HNO_3, are not important under tropospheric conditions. Heterogeneous loss of HONO on various surfaces is too slow to be relevant in most cases (Stutz et al., 2002, and references therein). During night, the ma-

jor HONO removal pathway is the dry deposition on ground surfaces (Trick, 2004), i.e.

$$\frac{d[HONO]}{dt} = \frac{v_{HONO}^{ground} \times [HONO]}{H} \qquad (1)$$

where v_{HONO}^{ground} is the deposition velocity of HONO and H the height of the well-mixed layer. The reported value of v_{HONO}^{ground} ranges from 0.077 to 3 cm s^{-1} (Harrison and Kitto, 1994; Harrison et al., 1996; Spindler et al., 1999; Stutz et al., 2002).

The question of HONO budget is two-fold, a day and a night problem. Due to the absence of solar radiation and low concentration of OH radicals during night, it is well accepted that the nocturnal HONO is mainly formed by the heterogeneous conversion of NO_2. Regardless the detailed chemical mechanisms, the strength of the HONO formation from NO_2 can be expressed as the HONO conversion frequency C_{HONO} (Alicke et al., 2002, 2003),

$$C_{HONO} = \frac{[HONO]_{t_2} - [HONO]_{t_1}}{(t_2 - t_1) \times \overline{[NO_2]}} \qquad (2)$$

where $\overline{[NO_2]}$ is the average NO_2 mixing ratio in the time interval of $t_2 - t_1$. In order to correct the effects of source emission and diffusion, complex scaling methods has been tested by Su et al. (2008a) during the calculation of C_{HONO}. They found that values of C_{HONO} derived from using different scaling species or without applying scaling method do not show a big difference.

During daytime, recent field observations find that the HONO concentration is too high to be explained by the gas phase Reactions (R1), (R2) and (R9). Therefore, the daytime HONO budget was expanded by an additional production rate term P_M (Su et al., 2008b).

$$\frac{d[HONO]}{dt} = \qquad (3)$$

$$k_{OH+NO}[OH][NO] + P_M - (J_{HONO} + k_{OH+HONO}[OH]) \times [HONO]$$

Here we omitted the influence of direct emission, deposition, horizontal and vertical transport on the HONO concentration since their influence is relatively small compared to the gas phase reactions and can be neglected in Eq. (3). Under quasi stationary conditions, i.e. $d[HONO]/dt \approx 0$, the additional production rate P_M can be expressed by

$$P_M = (J_{HONO} + k_{OH+HONO}[OH]) \times [HONO] - k_{OH+NO}[OH][NO] \quad (4)$$

which also corresponds to an additional HONO concentration $[HONO]_M$ calculated from from the difference of the measured HONO and the budget without P_M:

$$[HONO]_M = [HONO] - \frac{k_{OH+NO}[OH][NO]}{k_{HONO+OH}[OH] + J_{HONO}} \qquad (5)$$

which is equivalent to

$$[HONO]_M = \frac{P_M}{k_{HONO+OH}[OH] + J_{HONO}} \qquad (6)$$

For the first time Kleffmann et al. (2005) had a full set of OH, NO, and photolysis frequency measurements simultaneously with HONO so they could directly derive P_M for their measurements in a mixed deciduous forest in Germany. Their value of $0.55\,\mathrm{ppb\,h^{-1}}$ exceeds the possible source by Reaction (R5) therefore indicating an additional source of HONO. Similar findings, using direct measurements of HONO, OH, NO, and J_{HONO}, were obtained by Acker et al. (2006b) and Wong et al. (2012).

With the fast economic growth, the Pearl River Delta (PRD) region in Southern China has been identified as one of the hot-spots of NO_2 by satellite measurements (Richter et al., 2005). The first continuous HONO measurements in the PRD region was conducted by Su et al. (2008a,b) at a non-urban site in XinKen ($22.61°$ N, $113.61°$ E). Besides the high nighttime HONO concentration (0.4–3.5 ppb) a surprisingly high daytime average of 1.2 ppb was observed. However, due to the lack of measured key parameters (i.e. photolysis frequencies and OH) and the low time resolution of their HONO measurement, the investigation of the daytime HONO chemistry by Su et al. (2008b) left some open questions. Here we present the HONO data recorded during the PRIDE-PRD2006 campaign. We performed 4 weeks of continuous HONO measurements at a rural site in PRD region by the LOPAP technique side-by-side to measurements of trace gases, HO_x radicals, aerosol parameters and meteorological conditions. The contribution of HONO to the HO_x production has been investigated and discussed by Lu et al. (2011). The relative contribution was found to be 8–28 % during the campaign. In this study, we are focusing on the analysis of the HONO budget. The simultaneous measurements that are used for the identification and quantification of HONO sources and sinks are summarized in Table 1.

2 Experiment

2.1 LOPAP instrument

HONO was measured by LOPAP (long path absorption photometer) technique which was pioneered by Kleffmann and co-workers (Heland et al., 2001; Kleffmann et al., 2006). The instrument used in this study was a commercial version of the original instrument (QUMA GmbH, Wuppertal). Since the LOPAP instrument has been described in detail previously we give only a short outline. Ambient air is sampled into a sampling unit consisting of two stripping coils in series. Stripping solution of 100 g sulfanilamide and 1 l HCl (37 % volume fraction) in 9 l MilliQ water is pumped through the coils. HONO and any interfering species in the sampled air will dissolve in the liquid phase forming NO_2^- followed by a rapid reaction of NO_2^- forming a stable diazonium salt. Almost all HONO and a small fraction of interfering species are taken out by the first coil, while the second coil takes out the same amount of interfering species but has no HONO

in it. After debubbling the remaining air, the formed diazonium salt solution of each coil is pumped from the sampling unit to the detection unit through a 2.5 m insolated Teflon tubing. Each solution is then reacted with a dye solution made by dissolving 1.6 g n-(1-naphthyl)-ethylenediamine-dihydrochloride in 8 l MilliQ water forming an azo dye. The concentration of the azo dye is monitored by a 2 channel optical absorption spectrometer which absorption cell consists of a 1.2 m long Teflon tubing (called Liquid Core Waveguide, LCW). Visible light from a white LED lamp (Lumileds, Typ: LUXEON V star white, LXHLLW6C) is focused into the tubing via fiber optics. At the opposite end of the LCW, the light is collected by a fiber and detected by the spectrometer. The absorption spectra are recorded on a computer for later data evaluation. All the processes above are continuously operated.

The sampled air flow and the liquid flow of the stripping solution was set to $1\,\mathrm{l\,min^{-1}}$ and $0.28\,\mathrm{ml\,min^{-1}}$, respectively, and both were calibrated every third day during the campaign. Zero measurements by sampling zero air were done manually every 12 h. With above settings, the sampling efficiency of HONO in the sampling unit was determined to be 99.93 %. The time resolution, detection limit and accuracy of the measurement was 5 min, 7 ppt and 10 %, respectively.

2.2 Measurement site and campaign setup

The PRIDE-PRD2006 intensive campaign took place from 3 to 31 July 2006 in the Pearl River Delta (PRD) area in Southern China. Our measurements were conducted at the Back Garden (BG) supersite ($23.50°$ N, $113.03°$ E) which is about 60 km northwest of Guangzhou. The BG site is located near a water reservoir and is surrounded by farmland (peanuts, lychees, trees, small forests). It experienced little local emissions from traffic, but road and building construction as well as biomass and cable burning were occasionally observed within the surrounding area. The campaign was within the framework of the Program of Regional Integrated Experiments of Air Quality over the Pearl River Delta (PRIDE-PRD2006, Zhang et al., 2012). This program targets on understanding the formation mechanism of O_3 and fine particulate matter within the densely populated PRD area.

The BG supersite was equipped with a comprehensive suite of atmospheric measurements (e.g. Garland et al., 2008; Hofzumahaus et al., 2009; Li et al., 2010; Lou et al., 2010; Lu et al., 2011). On-site measurements used in this study are reported in Table 1 with their time resolutions and positions relative to the LOPAP. The sampling unit of the LOPAP was fixed on the top of the FZJ lab container housing the HO_x (Lu et al., 2011) and OH reactivity (Lou et al., 2010) instruments. The container was stacked on top of a second container hence the sampling height was 6 m above the ground. The detection unit (i.e. pumps, spectrometers etc.) was placed inside the lab container which was held at constant temperature.

Table 1. Instrumentation at the Guangzhou backgarden supersite. The instruments listed here do only refer to data used in this study. For a comprehensive overview of all instruments participating see Hofzumahaus et al. (2009); Lou et al. (2010); Lu et al. (2011); the measured parameters are explained in the text.

Instrument	Parameter	Group	Time res.	Position	Distance[a]	Reference
LOPAP	HONO	FZJ	1 min	top of LIF container	–	this work
LIF[b]	OH	FZJ	1 min	top of LIF container	1 m	Lu et al. (2011)
LP-LIF[c]	k_{OH}	FZJ	1 min	top of LIF container	1 m	Lou et al. (2010)
CL[d]	NO, NO_2	UT	1 min	hotel roof	200 m	Takegawa et al. (2006)
SR[e]	J_{HONO}, J_{NO_2}, J_{HNO_3}	FZJ	1 min	hotel roof	200 m	Bohn et al. (2008)
GAC-IC[f]	HNO_3	PKU	30 min	hotel roof	200 m	Su et al. (2008b)
TDMPS-APS[g]	S_a	IfT	10 min	hotel roof	200 m	Yue et al. (2010)
NEPH+PAS[h]	$\sigma_{a,532}$, ω_{532}	MPIC	2 min	hotel roof	200 m	Garland et al. (2008)
MET[i]	RH	PKU	10 min	hump at LIF container	20 m	Hofzumahaus et al. (2009)

[a]: horizontal distance from inlet to HONO sampling. The sampling height on top of the LIF container was 6 m less than on the hotel roof. [b]: Laser Induced Fluorescence. [c]: Laser-flash Photolysis Laser Induced Fluorescence. [d]: Chemiluminescence. [e]: Spectro radiometer. [f]: Gas and aerosol collector followed by Ion Chromatograph detection. [g]: Twin Differential Mobility Particle Sizer and Aerodynamic Particle Sizer. [h]: Nephelometer and Photoacoustic spectrometer. [i]: Meteorology station.

OH concentrations were measured by laser induced fluorescence (LIF) spectroscopy (Hofzumahaus et al., 2009; Lu et al., 2011). Ambient air was sampled by gas expansion into a low-pressure (3.5 hPa) fluorescence cell, where the OH radicals were electronically excited by tunable, pulsed UV laser radiation at a wavelength of 308 nm. The resulting OH resonance fluorescence was detected by time-delayed gated photon counting. The limit of detection was $(0.5–1) \times 10^6\,\text{cm}^{-3}$ at 5 min integration time and the accuracy was 20 % (1σ). The laser of the LIF was also used for the OH reactivity instrument (Lou et al., 2010) which was setup in the same container. This instrument provided OH reactivities in the range between $1\,\text{s}^{-1}$ and $100\,\text{s}^{-1}$ at 1 min time resolution.

NO and NO_2 were measured by commercial instruments (Takegawa et al., 2006). NO was detected by $NO-O_3$ chemiluminescence (Thermo Electron, Model 42CTL), while NO_2 was first converted to NO in a photolytic reactor (Droplet Measurement Technologies, Model BLC). The 1 min detection limits for NO and NO_2 were 50 ppt and 170 ppt, respectively, and the corresponding accuracies were 7 % and 13 %. However, during the campaign the instruments were stopped occasionally for repair and maintenance. The gaps (less than 10 % of the data set) were filled with data of a second instrument operated by PKU at the BG site.

The aerosol surface density S_a was calculated from the particle number size distributions between 3 nm and 10 µm by assuming the particles are in spherical shape (Yue et al., 2010). The particle number size distributions were measured by a system consisting of a Twin Differential Mobility Particle Sizer (TDMPS) and an APS (TSI model 3321). The relative humidity within the whole system was kept below 30 % by silica gel tubes within the inlet line and both sheath air cycles. The accuracy of derived S_a was estimated to be around 20 %. A hygroscopic factor $f(\text{RH})$ was applied to correct S_a to the aerosol surface density in the real atmosphere (S_{aw}).

$$f(\text{RH}) = 1 + a \times \text{RH}^b \tag{7}$$

$$S_{aw} = S_a \times f(\text{RH}) \tag{8}$$

The empirical factors a and b used to estimate $f(\text{RH})$ were set to 2.06 and 3.6, respectively, as described by Liu et al. (2008).

Total aerosol particle scattering coefficients ($\sigma_{s,\lambda}$) and hemispheric backscattering coefficients ($\sigma_{bs,\lambda}$) at three different wavelengths ($\lambda = 450\,\text{nm}$, 550 nm, and 700 nm) were measured by an integrating nephelometer (Model 3563, TSI). The aerosol particle absorption coefficient at 532 nm ($\sigma_{a,532}$) was determined with a photoacoustic spectrometer (PAS; Desert Research Institute), which provides highly sensitive absorption measurements without interference by scattering signals. These two instruments shared the same PM_{10} inlet with the TDMPS-APS system, and thus provided data at ≈ 30 % relative humidity. The accuracy of the nephelometer and the PAS data was 10 %. The aerosol single scattering albedo at 532 nm (ω_{532}) was calculated as the ratio of the interpolated $\sigma_{s,532}$ and measured $\sigma_{a,532}$ (Garland et al., 2008).

Gaseous nitric acid, HNO_3, was measured by a GAC-IC system (Su et al., 2008b). The system consists of a gas and aerosol collector (GAC) and an ion chromatograph detector (IC). The GAC uses an annular wet denuder to collect HF, HCl, SO_2, HONO, HNO_3 in gas phase and F^-, Cl^-, SO_4^{2-}, NO_2^-, NO_3^- in $PM_{2.5}$. The ambient air was sampled into the denuder through a 6 m Teflon tube with an air flow rate of $16.7\,\text{l}\,\text{min}^{-1}$. The stripping solution used in the denuder was $25\,\mu\text{mol}\,\text{l}^{-1}$ Na_2CO_3. The time resolution for all species was 30 min, while the detection limits for HNO_3 and aerosol nitrate were 65 ppt and $0.4\,\mu\text{g}\,\text{m}^{-3}$, respectively.

Photolysis frequencies were calculated from solar actinic-flux spectra recorded by a spectroradiometer (Meteorologie

Consult) as described by Bohn et al. (2008). The accuracy of the HONO photolysis frequency, J_{HONO}, was estimated to be 10 % at solar zenith angles smaller than 80°.

Wind speed and temperature were measured by an ultrasonic anemometer (USA-1, Metek, Germany) on the top of the lab container. A weather station (WXT510, Vaisala, Finland) was located on a small elevation behind the container (20 m distance). The accuracies for temperature, relative humidity, and pressure were 0.3 K, 3 %, and 0.5 hPa, respectively.

3   Results

We performed nearly continuous HONO measurements from 3 to 26 July 2006 (Fig. 2). HONO exhibits a clear diurnal cycle with peaks in the early morning and minima around noontime. The nighttime maxima ranged from 1 ppb to 5 ppb. Especially during two days (24 and 25 July) when intense electric cable combustion events happened, the nocturnal HONO concentration exceeded 4 ppb in the early morning hours. During an extended rainfall period (15 to 18 July, influence of typhoon Bilis) the concentration of HONO as well as other trace species were at their lowest level of the campaign. When we average the entire data set the mean maximum HONO concentration was 1.5 ppb, occurring around sunrise (Fig. 3b). The average HONO mixing ratio at noon time was about 200 ppt, however with large variations between 10 ppt and 490 ppt (Fig. 3b).

The entire campaign was characterized by tropical conditions with high temperatures (28–36 °C) and high humidities between 60 % and 95 % relative humidity (Fig. 2). The rainfall period (Typhoon Bilis) is clearly seen in the relative humidity record with constant values above 90 % throughout the day. It is also represented in the solar radiation which is strongly reduced as shown by the photolysis frequency of HONO (J_{HONO}) and NO₂ (J_{NO_2}). At the field site, local wind speeds were generally slow and had values mostly less than $2 \, m \, s^{-1}$ measured at 8 m height directly above the HONO inlet. These conditions correspond to the typical summer weather condition in the PRD region. The general weather pattern consists of high temperatures, high humidities, and dense cloud cover as reported by Chan and Yao (2008). The prevailing geostrophic winds are from the southeast, south and southwest due to the monsoon circulation. The typical ground wind speed at inland locations is around $1.5 \, m \, s^{-1}$, a situation which favors the accumulation of air pollutants.

Figure 2 also presents the time series of simultaneously measured trace gases and aerosol parameters. Noontime OH concentrations reach $(1–2) \times 10^7 \, cm^{-3}$ on every day when OH data were reported. However, the LIF instrument could not be operated during the rainfall period due to technical problems. The measured OH reactivity (k_{OH}) record indicates the high level of reactants present. Combining OH concentrations and reactivities show the enormous turnover
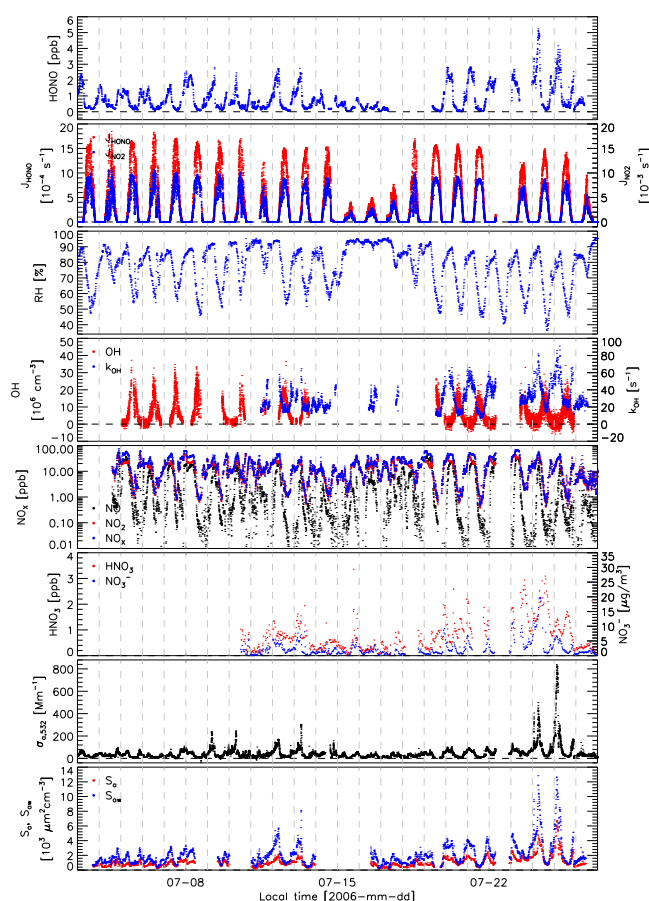
Fig. 2. Time series of HONO, J_{HONO}, J_{NO_2}, RH, OH, k_{OH}, NO, NO₂, NO$_x$, gas phase HNO₃, aerosol light absorption ($\sigma_{a,532}$), aerosol surface density (S_a) and RH corrected aerosol surface density (S_{aw}) at the Back Garden supersite in July 2006.

under these conditions (Hofzumahaus et al., 2009). At the same time the levels of NO and NO₂ show a large variability. Maximum mixing ratios of NO, NO₂, and NO$_x$ were 20 ppb, 30 ppb, and 50 ppb, occurring in the early morning when all ozone has been titrated by NO emissions. The gas phase HNO₃ concentrations are in the range of 100 ppt to 3 ppb with an average of 700 ppt, which are comparable with those observed at other rural sites (e.g. Zhou et al., 2007). Similar variations can be found between HNO₃ and HONO.

In contrast to the gas phase parameters shown here, the aerosols exhibit a less pronounced diurnal variation, as demonstrated by the aerosol surface density (S_a and S_{aw}) and aerosol light absorption ($\sigma_{a,532}$) in Fig. 2. The major variation comes from the different pollution levels, namely the burning events at the end of the campaign. The elevated values strongly reduced the visibility to values in the order of 1–2 km. The aerosol surface density and aerosol light absorption show a very similar pattern. Therefore, the aerosol light absorption can fill gaps in the aerosol surface density record, i.e. in the rainfall period.

Table 2. Overview on HONO measurements performed in or in the vicinity of big cities. The daytime values correspond to ± 3 h around local noon, the nighttime values reperesent averages between sunset and sunrise.

Location	Date	HONO [ppb]		NO$_2$ [ppb]		NO$_x$ [ppb]		HONO/NO$_2$		HONO/NO$_x$		Ref.
		night	day	night	day	night	day	night	day	night	day	
Santiago (Chile)	Mar 2005	3.00	1.50	30.0	20.0	200.0	40.0	0.100	0.075	0.015	0.038	1
Guangzhou (China)	Jun 2006	3.50	2.00	20.0	30.0	n.a.[d]	n.a.	0.175	0.067	n.a.	n.a.	2
Seoul (Korea)	May–Jul 2005	0.36	0.36	56.0	56.0	n.a.	n.a.	0.006	0.006	n.a.	n.a.	3
Kathmandu (Nepal)	Jan–Feb 2003	1.74	0.35	17.9	8.6	20.1	13.0	0.097	0.041	0.087	0.027	4
Taichung (Taiwan)	Jul–Jan 2005/2006	1.50	0.50	25.0	16.7	n.a.	n.a.	0.060	0.030	n.a.	n.a.	5
Xinken (China)	Oct–Nov 2004	1.30	0.80	34.8	30.0	37.8	40.0	0.037	0.027	0.034	0.020	6
Rome (Italy)	May–Jun 2001	1.00	0.15	27.2	4.0	51.2	4.2	0.037	0.038	0.020	0.036	7
Milan (Italy)	May 1998	0.92	0.14	33.2	18.3	117.5	23.4	0.028	0.008	0.008	0.006	8
Shanghai (China)	Oct–Jan 2004/2005	1.50	0.35	26.0	16.0	n.a.	n.a.	0.058	0.022	n.a.	n.a.	9
Tokyo (Japan)	Jan–Feb 2004	0.80	0.05	31.8	18.2	37.4	26.3	0.025	0.003	0.021	0.002	10
Mexico City (Mexico)	Mar 2006	n.a.	0.43	n.a.	28.4	n.a.	44.8	n.a.	0.015	n.a.	0.010	11
Pabstthum[a] (Germany)	Jul–Aug 1998	0.33	0.07	2.9	3.6	3.3	4.6	0.112	0.018	0.099	0.014	12
Yufa[b] (China)	Jul–Aug 2006	0.89	0.43	14.2	8.0	18.3	9.4	0.062	0.054	0.048	0.046	13
Houston (USA)	Sep 2006	0.5	0.1	20.0	10.0	n.a.	n.a.	0.025	0.010	n.a.	n.a.	14
Backgarden[c] (China)	Jun 2006	0.95	0.24	16.5	4.5	20.9	5.5	0.057	0.053	0.045	0.043	–

[a]: near Berlin. [b]: near Beijing. [c]: near Guangzhou. [d]: not available. 1: Elshorbany et al. (2009); 2: Qin et al. (2009); 3: Song et al. (2009); 4: Yu et al. (2009); 5: Cheng et al. (2008); 6: Su et al. (2008a,b); 7: Acker et al. (2006a); 8: Alicke et al. (2002); 9: Hao et al. (2006); 10: Kanaya et al. (2007); 11: Dusanter et al. (2009); 12: Alicke et al. (2003); 13: Yang et al. (2010); 14: Wong et al. (2011).
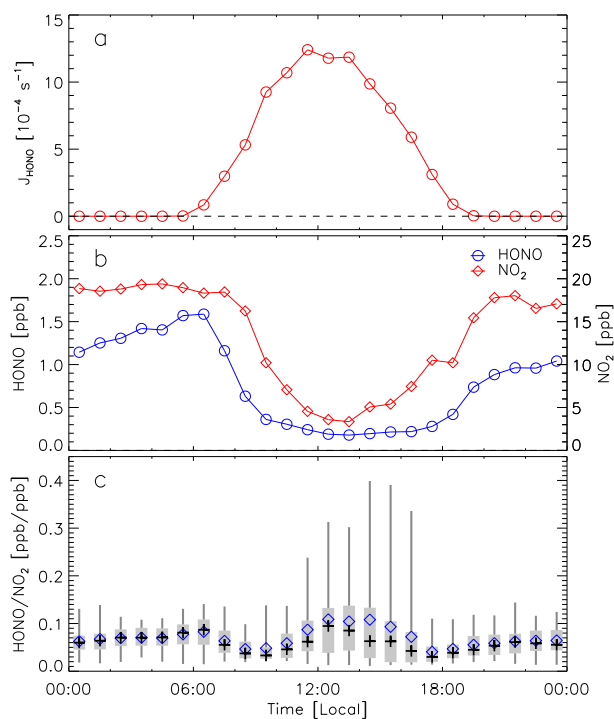
Fig. 3. Mean diurnal cycle of J_{HONO}, HONO, NO$_2$ and HONO/NO$_2$ at the Back Garden supersite in July 2006. In **(c)**, the + refers to the median, boxes represent 50 % (25 % to 75 %), the whiskers 90 % of the data. The blue diamond is the average.

4 Discussion

### 4.1 HONO concentrations and the influence of direct HONO emissions

The observed HONO concentrations with maximum values above 5 ppb at night and of 200 ppt at overhead sun (Fig. 2) are among the highest ever recorded at a site outside of big cities (cf. Alicke et al., 2003; Kleffmann et al., 2005; Cheng et al., 2007; Shon et al., 2007; Zhou et al., 2007). However, when we refer to campaign averages and relate them to measurements which were done in or in the vicinity of big cities (Table 2) we see that the BG data are at the low end for nighttime and almost average for daytime observations. Our nighttime values compare to Beijing and Tokyo values, while daytime mixing ratios are lower than other observations in Asia. In order to relate the HONO concentration to the level of local pollution and the possible HONO sources, the HONO to NO$_2$ and/or the HONO to NO$_x$ ratio has been used in many publications to create a more stable value for charactering the level of HONO.

The ratio HONO/NO$_2$ has the advantage of being less influenced by convection or transport processes than individual concentrations and it can be used to indicate the heterogeneous conversion efficiency of NO$_2$ to HONO. However, when a large fraction of HONO comes from direct emissions the ratio might be influenced. Emission ratios of HONO to NO$_2$ were measured to be less than 1 % as reported by Kurtenbach et al. (2001, and references therein).

Considering the conversion from NO_2 to HONO, higher value of $HONO/NO_2$ can be expected for an aged air mass. The $HONO/NO_2$ observed in many field studies range from 2 % to 10 % with lower values in the fresh air masses (Febo et al., 1996; Lammel and Cape, 1996; Alicke et al., 2002, 2003; Stutz et al., 2004; Zhou et al., 2007; Su et al., 2008b; Sörgel et al., 2011b). The measured $HONO/NO_2$ during the PRIDE-PRD2006 campaign ranged from <1.1 % (1 % quantile) to >35 % (99 % quantile) with mean value of 7.1 ± 6.1 %. The recorded $HONO/NO_2$ greater than 35 % exceed the ever reported highest ratio by Yu et al. (2009) (i.e. 30 % during 00:00–03:00 LT at Kathmandu). However, different from Yu et al. (2009), the high ratios obtained by us always occurred during 12:00–15:00 LT.

Figure 3c displays the mean diurnal variation of $HONO/NO_2$ at the BG site. In general, the highest ratios with large variability were found from 11:00 to 17:00 LT, even higher than those during the nights. This can be attributed to the efficient daytime formation of HONO which is not correlated to NO_2 (see Fig. 9 and the discussion about the additional HONO source below). On average, $HONO/NO_2$ started to increase shortly after sunset and kept stable at ≈ 6 % in the rest of the night. The increase of $HONO/NO_2$ was accompanied by the simultaneous increase of HONO and NO_2, suggesting the heterogeneous conversion from NO_2 to HONO. Once the conversion reached a steady state, the $HONO/NO_2$ became stable. The covariation between HONO and NO_2 during nighttime (19:00–06:00 LT) can further be seen from the correlation plot (Fig. 4b), indicating NO_2 as the precursor of HONO in this time interval. Figure 4b also shows the dependence of the $HONO/NO_2$ ratio on the aerosol surface density (S_{aw}) during night. Higher values of $HONO/NO_2$ are usually found at higher levels of S_{aw}, suggesting the possible influence of aerosol surfaces on the heterogeneous NO_2 to HONO conversion. However, as will be discussed later, compared to the ground surfaces, the influence of aerosol surfaces on the HONO formation is small. The nighttime stable $HONO/NO_2$ values were slightly higher than that observed by Su et al. (2008a) (4.3 ± 1.5 %) in the same region. The decrease of $HONO/NO_2$ can be caused by emissions or transport. The increase of $HONO/NO_2$ and its high value during daytime suggests a high HONO formation efficiency, which however might not be solely explained by the NO_2 conversion given the weak correlation between HONO and NO_2 (Fig. 4a). Moreover, as higher $HONO/NO_2$ ratios are usually found at lower RH level (Fig. 4a), the daytime HONO formation is unlikely caused by Reaction (R5). As will be discussed later, additional HONO production mechanisms are needed to sustain the high daytime level of HONO as well as $HONO/NO_2$.

As the BG site was characterized by occasional local emissions from biomass and electric cable burning processes, it is necessary to separate HONO formed by chemical reactions from directly emitted. Emission factors of HONO are only available for vehicles obtained through either tun-
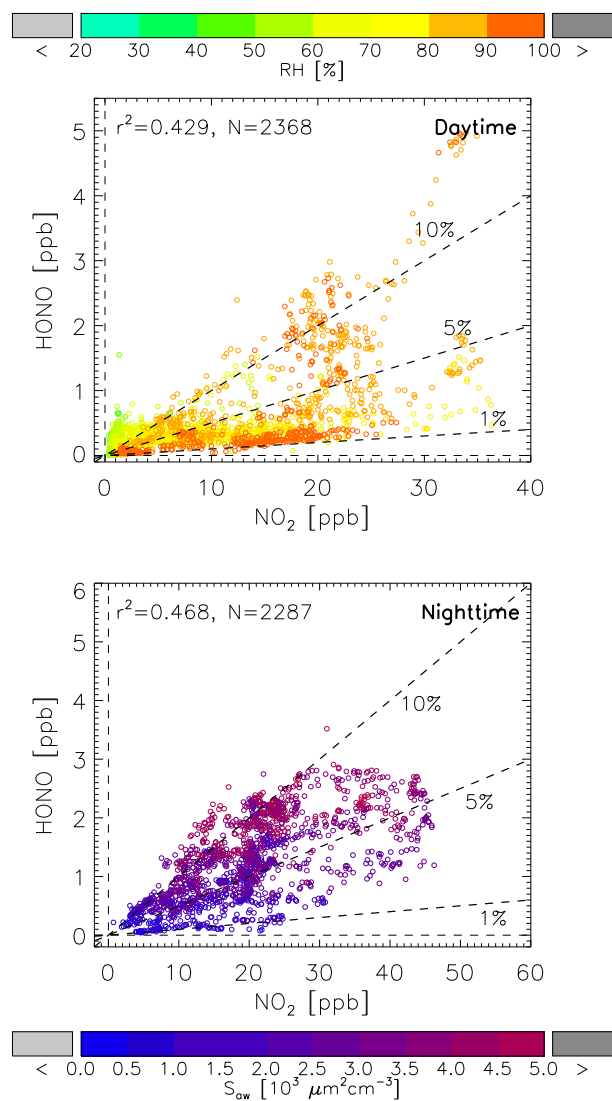

Fig. 4. Correlation between HONO and NO_2. The dashed lines correspond to the $HONO/NO_2$ ratio of 10 %, 5 % and 1 %. The nighttime data are in the time period of 19:00–06:00 LT and color coded by the aerosol surface density; while the daytime data are color coded by the relative humidity.

nel experiments or laboratory studies in the US and Europe (Kurtenbach et al., 2001, and references therein). Considering the differences in combustion processes, fuel compositions, etc., the reported emission of HONO relative to NO_x (i.e. $HONO/NO_x$) might not be representative for PRD region. In order to evaluate the influence of direct emissions, we tried to estimate the local HONO emission factor from the ambient measurements.

When the air mass is getting aged, due to the conversion from NO_2 to HONO, the $HONO/NO_x$ ratio will increase; the freshly emitted air mass should have the lowest $HONO/NO_x$. Thus, we used the observed lowest $HONO/NO_x$ as the upper limit for the emission factor. Besides, two other filters as
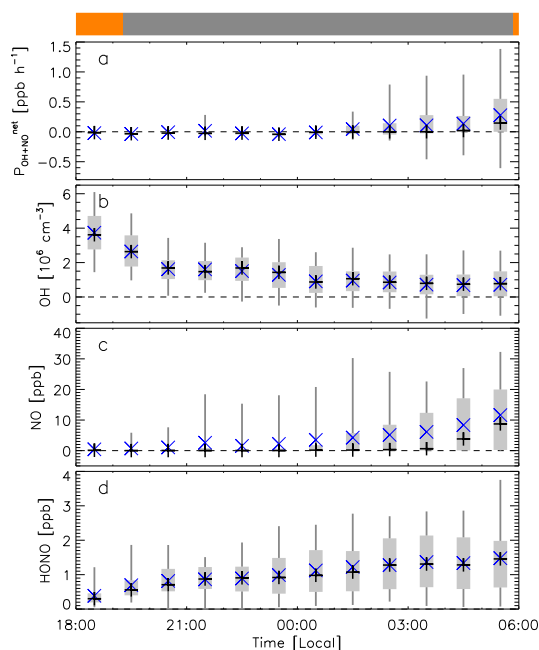
Fig. 5. Mean nocturnal variation of P_{OH+NO}^{net}, OH, NO and HONO. The color bar illustrates the local day (orange) and night (grey). These box-whisker diagram are based on 1 h averages for time intervals where both measurements were present. The + refers to the median, boxes represent 50 % (25 % to 75 %), the whiskers 90 % of the data. The blue × is the average.

proposed by Su et al. (2008a) were applied: (1) only nighttime data were included in order to avoid the fast photolysis of HONO; (2) NO ≥ 20 ppb was used to catch the fresh emissions. The derived $HONO/NO_x$ is 1.8 % much higher than 0.8 % reported by Kurtenbach et al. (2001). During the experiments conducted by Kurtenbach et al. (2001), air masses were characterized by $NO/NO_x \geq 95\%$. The typical NO/NO_x ratio in our measurements is ≈50 %, suggesting the air detected is a mixture of freshly emitted and aged. Therefore, a substantial part of HONO is secondary. Since the observed NO/NO_x and $HONO/NO_x$ during the entire campaign period has an average of 13 % and 6 %, respectively, the influence of direct emissions on HONO should be small and hence be ignored in the following analysis.

4.2 HONO during night

The nocturnal pattern observed here is similar to ever reported: HONO increases after sunset to a maximum at sunrise. Since most of the dynamic range of the HONO concentration is during the night, the correlation between HONO and NO_2 is mostly created during nighttime hours. In this section, we will focus on the formation pathways of the nocturnal HONO and explore the relevant factors.

### 4.2.1 Gas phase formation through OH + NO

During the PRIDE-PRD2006 campaign, a substantial measured OH concentration of $\approx 1 \times 10^6$ cm^{-3} together with NO mixing ratios larger than 2 ppb were found in the night (Fig. 5b, c), which brings up the importance of OH + NO on the nighttime HONO formation. Taking Reactions (R2) and (R9) into account, the net HONO production is

$$P_{OH+NO}^{net} = k_{OH+NO}[OH][NO] - k_{OH+HONO}[OH][HONO] \quad (9)$$

The mean nocturnal variation of P_{OH+NO}^{net} is illustrated in Fig. 5a. Since k_{OH+NO} and $k_{OH+HONO}$ are similar (7.2 and 5.0 in units of 10^{-12} cm^3 s^{-1} at 298 K), the P_{OH+NO}^{net} depends on the relative abundance of NO and HONO. Before midnight, due to the low NO level, small negative value of P_{OH+NO}^{net} was found. The formation of HONO in this time period might mostly come from the NO_2 conversion as will be discussed later. After midnight, with the sharp increase of NO mixing ratios, the P_{OH+NO}^{net} increased from 0 to 0.28 ppb h^{-1}. Higher P_{OH+NO}^{net} of 0.4–0.9 ppb h^{-1} were found by Wong et al. (2011) for the nocturnal urban atmosphere of Houston. By integrating P_{OH+NO}^{net} from 00:00 to 06:00 LT, an accumulated HONO formation of 0.66 ppb can be derived. However, the averaged measured HONO accumulation in this time period was only 0.36 ppb. This suggested that, (1) the reaction of OH + NO is enough to explain the increase of HONO in the second half of the night, even though sources like NO_2 conversion might still existed; (2) the strength of HONO sinks other than OH + HONO should be at least in the order of 0.05 ppb h^{-1} (i.e. (0.66 ppb − 0.36 ppb)/6 h).

4.2.2 Heterogeneous conversion of NO_2

Figure 6 illustrates the correlation between HONO, $HONO/NO_2$, RH corrected aerosol surface density from 3 nm to 10 µm (S_{aw}) and aerosol light absorption at 532 nm ($\sigma_{a,532}$). As the HONO production by OH + NO was prominent in the second half of the night, we restrict the correlation analysis to the time frame 18:00–0:00 LT. Both HONO and $HONO/NO_2$ increase with S_a and $\sigma_{a,532}$. Compared with $HONO/NO_2$, HONO has better correlation with S_{aw} and $\sigma_{a,532}$, which was probably due to the decrease of boundary layer height leading to the simultaneous concentration change of trace gases and aerosols. Whilst this effect can largely be canceled out in the $HONO/NO_2$. The positive correlation between $HONO/NO_2$ and S_{aw} indicates the HONO formation on aerosol surfaces through the heterogeneous conversion of NO_2, which has already been found in Fig. 4b. However, considering the correlation is weak ($r^2 = 0.184$), the relative amount of HONO formed on aerosol surfaces might be small. The $\sigma_{a,532}$ provides the information of black carbon or soot content in the atmosphere. The even weaker correlation between $HONO/NO_2$ and $\sigma_{a,532}$ indicates a small
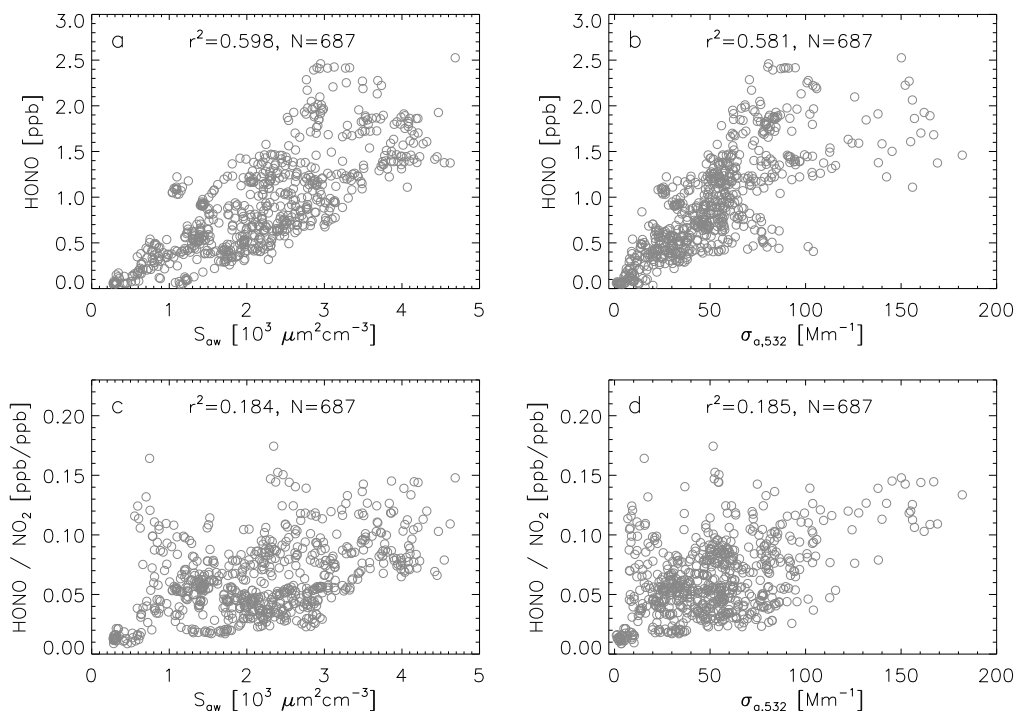
Fig. 6. Correlations between HONO/NO$_2$, HONO, aerosol surface density (RH corrected), aerosol light absorption during the time interval of 18:00–00:00 LT.
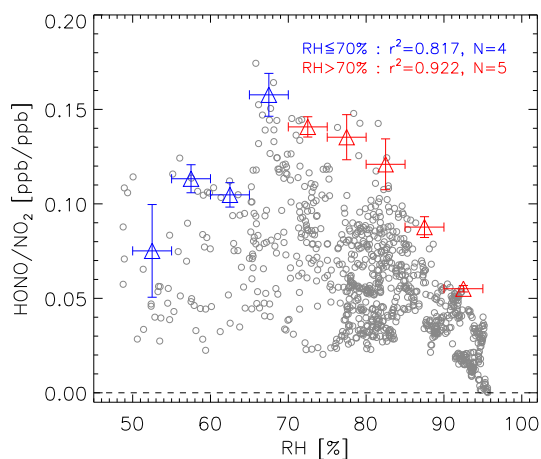
Fig. 7. Scatter plot of HONO/NO$_2$ against RH in the time interval of 18:00–00:00 LT (time interval avoids influence of OH+NO, see Fig. 5). Triangles are the averaged top-5 HONO/NO$_2$ in each 5 % RH interval.

role of soot in the heterogeneous HONO formation. The relationship between HONO/NO$_2$ and relative humidity RH is illustrated in Fig. 7. Following the method introduced by Stutz et al. (2004), we analyzed the top-5 HONO/NO$_2$ values in each 5 % RH interval. These are less influenced by factors like the time of the night, the surface density, advection, etc. The dependence of HONO/NO$_2$ on RH can be divided into two groups. An increase of HONO/NO$_2$ along with RH was found when RH was less than 70 %, which is consistent with the kinetics of Reaction (R5). Once RH was higher than 70 %, the NO$_2$ to HONO conversion efficiency depended negatively on RH. The same phenomenon was also observed by Yu et al. (2009) in Kathmandu. This finding can be associated with the number of water layers formed on various surfaces increases rapidly with relative humidity, leading to an efficient uptake of HONO. Thus HONO is lost in the gas phase when on the surface loss becomes dominant (Lammel, 1999; Stutz et al., 2004).

Using the data from the first half of the night (18:00–00:00 LT), we calculated the HONO conversion frequency C_{HONO} by Eq. (2). The average value of C_{HONO} during the campaign was $0.024 \pm 0.015\,h^{-1}$, corresponding to a HONO production rate by NO$_2$ (P_{NO_2}) of $0.38 \pm 0.25\,ppb\,h^{-1}$ (i.e. $C_{HONO} \times \overline{[NO_2]}$). It is necessary to note that, (1) the C_{HONO} assumes all the measured HONO is coming from the conversion of NO$_2$; and (2) the derived P_{NO_2} is the net HONO production, which means sinks of HONO (e.g. deposition, HONO + OH, etc.) have already been taken into account in P_{NO_2}. The HONO conversion frequency obtained in this work is comparable to observations of Su et al. (2008b) in the same region ($0.016 \pm 0.014\,h^{-1}$) and by Alicke et al. (2003) at a rural site in Pabstthum ($0.018 \pm 0.009\,h^{-1}$), but much higher than observation at other places (e.g. Lammel, 1999; Alicke et al., 2002; Acker et al., 2005; Sörgel et al., 2011a,b).

The formation of HONO through heterogeneous NO_2 conversion on aerosol surfaces (S_{aw}) depends on many factors and can be approximated by

$$P_{hetero} = \frac{1}{4} \gamma_{NO_2 \to HONO} \times S_{aw} \times v_{NO_2} \times [NO_2] \quad (10)$$

where $\gamma_{NO_2 \to HONO}$ is the uptake coefficient of NO_2 to HONO, and v_{NO_2} the mean molecular velocity of NO_2 (Ammann et al., 1998). If the entire HONO formation were taking place on aerosol surfaces of with density S_{aw}, $\gamma_{NO_2 \to HONO}$ calculated from Eqs. (2) and (10) would have an average of $(2.8 \pm 1.5) \times 10^{-5}$. Using the measured single scattering albedo at 532 nm ω_{532}, and considering the soot particles are usually hydrophobic, the soot surface density can be roughly estimated as $S_{soot} = (1 - \omega_{532}) \times S_a$. Further assuming all HONO was formed on soot surfaces, the average value of $\gamma_{NO_2 \to HONO}^{soot}$ was found to be $(3.0 \pm 1.8) \times 10^{-4}$. As discussed by Kleffmann et al. (1998), this value seems too high for ambient aerosols. Especially for soot particles, along with the air mass is getting aged, the $\gamma_{NO_2 \to HONO}^{soot}$ will decrease dramatically to a value which is in the order of 10^{-5} (Aubin and Abbatt, 2007). Moreover, given the weak correlation of NO_2 to HONO conversion efficiency against S_{aw} and $\sigma_{a,532}$, we conclude that the HONO production was mostly taking place at ground surfaces rather than aerosols during nighttime. These ground surfaces could include the surfaces of plants, buildings, soils and so on in surrounding areas which can typically provide orders of magnitude higher surface density than aerosols (Sörgel et al., 2011b). A similar conclusion was drawn from recent studies in both forest and urban areas (Sörgel et al., 2011b; Wong et al., 2011).

4.2.3 Removal of HONO through deposition

In Sect. 4.2.1, we mentioned that the production of HONO estimated from gas phase reactions (i.e. Reactions (R2) and (R9)) was larger than that from the measurement. Moreover, as the heterogeneous NO_2 conversion can also take place in the second half of the night, this discrepancy will become even larger. Assuming a constant C_{HONO} over night and the extra HONO are all removed through deposition on the ground, the HONO deposition velocity v_{HONO}^{ground} can be roughly estimated by,

$$\frac{d[HONO]}{dt} = P_{OH+NO}^{net} + C_{HONO} \times \overline{[NO_2]} - \frac{v_{HONO}^{ground} \times [HONO]}{H} \quad (11)$$

The v_{HONO}^{ground} calculated from the mean nocturnal variation (00:00–06:00 LT in Fig. 5) is $\approx 0.8 \, cm \, s^{-1}$ taken the night time H of 100 m. This value is substantially higher than observations by Stutz et al. (2002) ($0.077 \, cm \, s^{-1}$) but within the range of other published results (0.5–$3 \, cm \, s^{-1}$) (Harrison and Kitto, 1994; Harrison et al., 1996; Spindler et al., 1999). The estimated high value of v_{HONO}^{ground} seems to be in line with the high RH during night which increases the water adsorbed at ground surfaces and favor the adsorption of HONO.

4.2.4 Formation of HONO on ground surfaces

As illustrated above, the nighttime HONO production was mainly from the heterogeneous NO_2 conversion on ground surfaces, which can be described as,

$$C_{HONO} = \frac{P_{HONO}}{[NO_2]} = \frac{\phi_{NO_2 \to HONO} \times v_{NO_2}^{ground}}{H} - \frac{v_{HONO}^{ground}}{H} \times \frac{[HONO]}{[NO_2]} \quad (12)$$

where $v_{NO_2}^{ground}$ and $\phi_{NO_2 \to HONO}$ is the dry deposition velocity of NO_2 and the yield of HONO from deposited NO_2, respectively (Su et al., 2008a). By definition, $\phi_{NO_2 \to HONO}$ varies between 0 and 1, accounting for the fact that the deposited NO_2 molecule is not necessarily converted to HONO. As the controlling resistances were the aerodynamic resistance and the quasi-laminar layer resistance during night, similar deposition velocities were expected for NO_2 and HONO. Thus, using the measured average value of C_{HONO}, NO_2, HONO and the estimated v_{HONO}^{ground}, and assuming a 100 m height of the well-mixed layer, a $\phi_{NO_2 \to HONO}$ value of 0.15 was found which means that one out of seven deposited NO_2 forms HONO being released into the atmosphere. Our derived $\phi_{NO_2 \to HONO}$ is lower than that by Su et al. (2008a) (0.34), which is mainly caused by using the different value of $v_{NO_2}^{ground}$ during the calculation.

4.3 Daytime HONO budget

The HONO data presented here were accompanied by simultaneous measurements of OH, NO, and J_{HONO}. Therefore, we can examine the HONO budget and HONO lifetime directly from measured quantities. The HONO chemical lifetime (τ_{HONO}) due to photolysis (Reaction R1) and reaction with OH (Reaction R9) was ≈ 50 min after sunrise and before sunset and decreased to ≈ 13 min under overhead sun conditions. Due to the short lifetime, especially around noon, HONO is in quasi steady state and we can calculate the budget of HONO from gas phase production and loss in the same way as Kleffmann et al. (2005) and Acker et al. (2006b) did for two rural sites in Germany. In order to justify the quasi steady state assumptions associated with Eqs. (4) and (5), we restricted the data set to $J_{HONO} > 8 \times 10^{-4} \, s^{-1}$. Under these conditions, the HONO lifetime was less than 20 min, and $d[HONO]/dt$ calculated from the measurements was small and evenly distributed around zero.

The P_M and $HONO_M$ (see Eqs. 4, 5, and 6) for the "high J subset" are shown in Fig. 8 (blue dots). The value of P_M was significantly higher than zero in most of the time, which corresponds to a substantial amount of $HONO_M$. Also shown in Fig. 8 are the mean diurnal variations of P_M, $HONO_M$ and measured HONO (open circles). The average P_M during the entire campaign period was $0.77 \pm 0.55 \, ppb \, h^{-1}$, which is comparable to observations by Kleffmann et al. (2005) in the forest in Jülich ($\approx 0.55 \, ppb \, h^{-1}$) and by Wong et al. (2012) in downtown Houston ($\approx 0.6 \, ppb \, h^{-1}$), but smaller than the estimation by Su et al. (2008b) in XinKen ($\approx 2 \, ppb \, h^{-1}$). Since
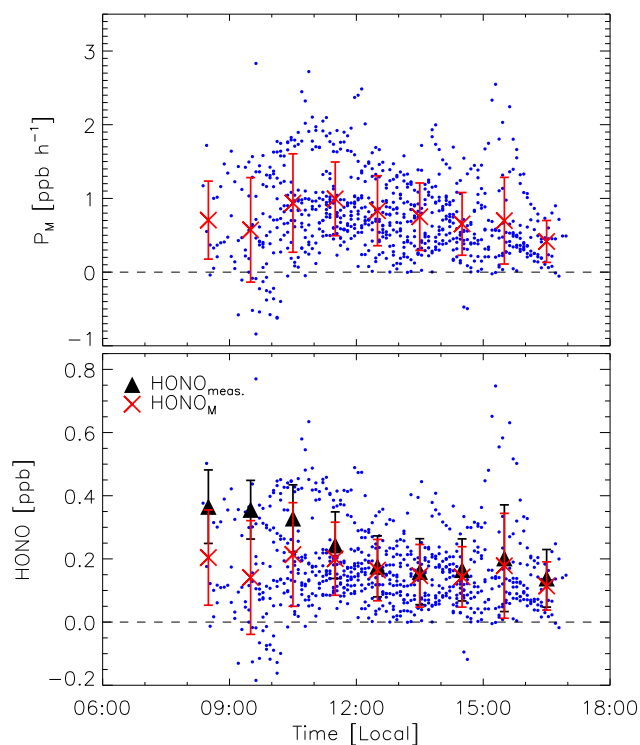
Fig. 8. Upper frame: Calculated additional HONO production rate P_M (Eq. 4). The blue dots correspond all 5-min averages where measurements of J_{HONO}, OH, NO and HONO were present. The red circles refer to the mean over 1 h with 1-σ error bars. Lower: additional HONO concentration $HONO_M$ (Eq. 5). Red circles are the mean values over 1 h, black triangles are the mean value of the measured HONO.

the daytime average minima of HONO in XinKen was as high as 1.2 ppb, higher value of P_M can be expected. P_M in the order of 0.1–2 ppb h^{-1} are also found in other rural and urban areas (Elshorbany et al., 2009; Ren et al., 2010; Sörgel et al., 2011a). The $HONO_M$ was the dominant part of measured HONO, accounting for >95 % since 11:00 LT. This means the daytime HONO formation was controlled by P_M while only a minor part (<5 %) came from gas phase OH + NO reaction.

Similar temporal variation pattern can be found between P_M and HONO/NO$_2$ (Fig. 3c). The simultaneous increase of P_M and HONO/NO$_2$ after 09:00 LT indicates either the elevated conversion efficiency from NO$_2$ to HONO or the existence of unknown HONO sources during daytime. Recent studies showed the heterogeneous NO$_2$ reaction forming HONO on various surfaces being photosensitive or photoenhanced (George et al., 2005; Stemmler et al., 2006). Therefore, higher HONO production rate can be expected when surfaces are exposed to sunlight. The production of HONO through the proposed mechanisms should be related to parameters including the gas phase NO$_2$ concentration, RH, aerosol/ground surface area density, soot/organic

composition on the surfaces, etc. The correlations of P_M against NO$_2$, RH, J_{NO_2}, S_{aw} and $\sigma_{a,532}$ do not provide a clear picture (Fig. 9). Relationship is neither found neither between P_M and J_{NO_2} nor between P_M and RH. According to Stemmler et al. (2006), the photosensitized HONO production will become saturated when the irradiance is above 200 W m^{-2}. Since our data are restricted to high J_{HONO} we did not explore the sensitive region in the laboratory study. A similar phenomenon was observed by Stemmler et al. (2007) with regard to RH, thus the range of humidities explored here might not be sensitive again. The correlation between P_M and NO$_2$ is two-fold. For NO$_2$ less than 4.5 ppb, a weak increase can be observed (Fig. 9a), while at higher NO$_2$ the values decrease (Fig. 9b). The higher NO$_2$ were only observed during the early morning (08:00–10:00 LT) and might caused by the NO to NO$_2$ conversion, the lower light levels and the lower boundary height.

The weak dependence of P_M on S_{aw} and $\sigma_{a,532}$ suggests the aerosol surfaces might not be the places where $HONO_M$ is formed. Even weaker relationship between P_M and parameters in Fig. 9 was found for individual measurement days except 24 July. The prevailing cable combustion events in surrounding areas happened during the night of 23 to 24 July. The high aerosol surface density and the soot concentration caused by the strong primary emissions could facilitate the HONO formation on aerosols. However, since the dependence of P_M on parameters in Fig. 9 is generally weak, we thought the contribution of heterogeneous NO$_2$ reaction to P_M should be quite small. To further prove our assumption, we calculated the $\gamma_{NO_2 \rightarrow HONO}$, $\gamma_{NO_2 \rightarrow HONO}^{soot}$, and $\phi_{NO_2 \rightarrow HONO}$ around noon (11:00–13:00 LT) by assuming P_M is only taking place on aerosol, soot particle and ground surfaces, respectively. The mean value of $\gamma_{NO_2 \rightarrow HONO}$ and $\gamma_{NO_2 \rightarrow HONO}^{soot}$ derived from Eq. (10) is 0.03 and 0.39, respectively. These values are three to four orders of magnitude higher than those obtained in laboratory studies. Using a mixing height of 250 m as suggested by Stemmler et al. (2006) and assuming the same dry deposition velocity between day and night, the mean value of $\phi_{NO_2 \rightarrow HONO}$ calculated by Eq. (12) is 135. This value is far away from the theoretical range (i.e. 0 to 1) and could not be explained by the uncertainty of v_{HONO}^{ground} ($v_{NO_2}^{ground}$). Therefore, we concluded that the contribution of heterogenous NO$_2$ reaction to P_M was quite small. Other HONO formation mechanisms are needed during daytime.

The photolysis of adsorbed HNO$_3$ on ground surfaces was suggested to be the major HONO source at Whiteface Mountain in the US (Zhou et al., 2003, 2007). As the adsorption of HNO$_3$ on ground surfaces occurs day and night, and the amount of adsorbed HNO$_3$ is proportional to the gas phase HNO$_3$ concentration, we correlated the average noontime P_M with the GAC-IC measured HNO$_3$ concentrations averaged over the previous 24 h period (Fig. 10a). A possitive correlation was found for the limited days when continuous
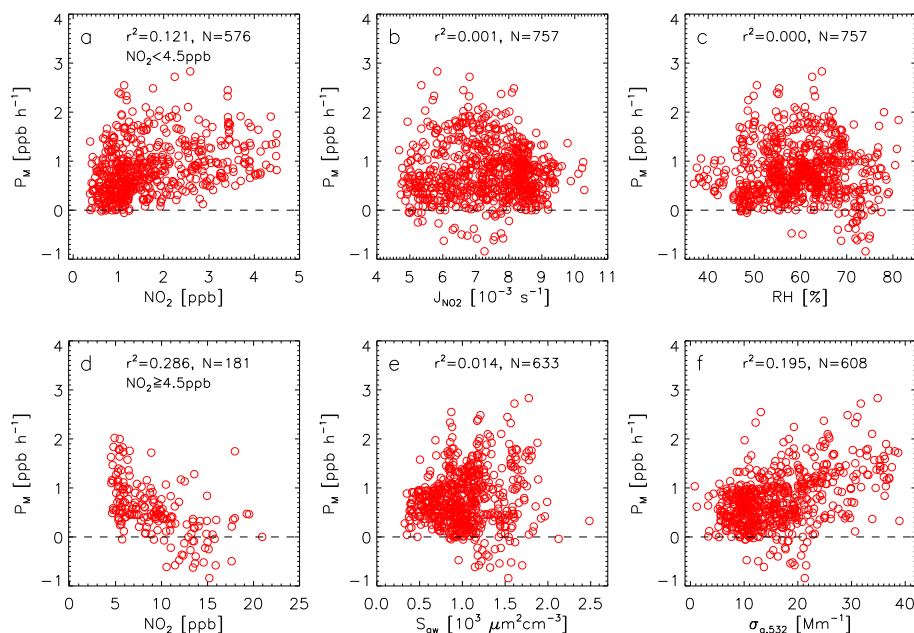
Fig. 9. Correlation of P_M against NO_2, J_{NO_2}, RH, S_{aw}, and $\sigma_{a,532}$.
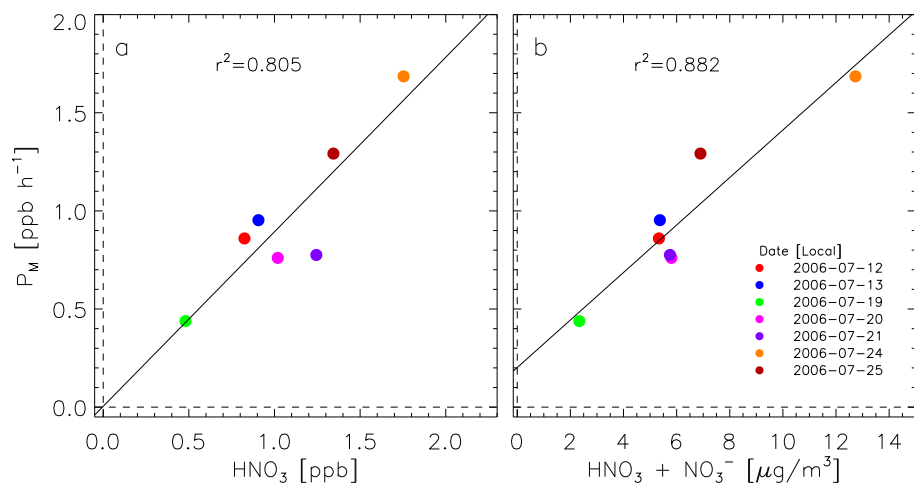
Fig. 10. Correlation of the average noontime (11:00–13:00 LT) additional HONO production rate (P_M) against the averaged HNO_3 concentration over the previous 24 h period **(a)** and the sum of the averaged HNO_3 and aerosol nitrate **(b)**. The seven data points are color-coded for the different days of the campaign. The slopes of the regression lines represent a parameterization of the HONO formation rate, see text for details.

HNO_3 measurements were available ($r^2 = 0.81$). The first-order approximation of production rate of HONO through this mechanism can be calculated as (Zhou et al., 2007),

$$P_{HNO_3 \rightarrow HONO} = \frac{f \times [HNO_3] \times \nu_{HNO_3} \times t_d \times j_{HNO_3 \rightarrow HONO}}{H} \quad (13)$$

where f is the fraction of noontime full sun to which the surfaces were exposed, ν_{HNO_3} is the dry deposition velocity of HNO_3 over t_d period, and $j_{HNO_3 \rightarrow HONO}$ the photolysis rate constant of HNO_3 via HONO pathway. Here, by assuming the surfaces containing HNO_3 within a mix-

ing height of 250 m were exposed to $f = 1/4$ noontime full sun, taking $\nu_{HNO_3} = 5 \, \text{cm s}^{-1}$ over $t_d = 24$ h, and using the average value of $P_M = 0.97 \, \text{ppb h}^{-1}$ and $[HNO_3] = 1.1$ ppb in Fig. 10a, the photolysis frequency $j_{HNO_3 \rightarrow HONO}$ derived from Eq. (13) was $5.7 \times 10^{-5} \, \text{s}^{-1}$. This value is comparable to measurments by Zhou et al. (2003) in the laboratory ($(1.2 \pm 0.2) \times 10^{-5} \, \text{s}^{-1}$). In addition, we also correlated the noontime P_M with the sum of the HNO_3 concentrations averaged over the previous 24 h period and the aerosol nitrate, both measured by GAC-IC (Fig. 10b). This scatter plot has

an even higher correlation ($r^2 = 0.88$) and the photolysis frequency $j_{\text{HNO}_3 \rightarrow \text{HONO}}$ of 2.5×10^{-5} s^{-1} is clsoer to the value obtained by Zhou et al. (2003). Given the good correlation of P_M with HNO$_3$ and the sum of HNO$_3$ and aerosol nitrate, we concluded that the photolysis of adsorbed HNO$_3$ on ground surfaces in surrounding areas could be one likely source for the missing daytime additional HONO formation. This is also supported the value of the calculated $j_{\text{HNO}_3 \rightarrow \text{HONO}}$.

Recently, Su et al. (2011) demonstrated that the soil nitrite, which is formed through the biological nitrification and denitrification processes, can be the source of HONO. The soil HONO emission (P_{soil}) was estimated to be 2–5 ppb h^{-1} for Xinken site. Since the BG site is surrounded by farmland, we can not exclude the possibility that the soil nitrite contributes to P_M. However, even if Xinken and BG are located in the same region, they represent different environments: Xinken is located at the southeast end of PRD around 200 km south of the Backgarden site. Xinken is at the seaside (at the Zhujiang river estuary) and located in a land reclamation area. However, the magnitude of the estimated P_{soil} covers our observed P_M. Since we did not measure the relevant information with regard to the nitrite concentration, the temperature, the pH value and the water content of the soil in the surrounding area during the campaign, it is difficult to quantify the P_{soil} and thus its contribution to P_M.

5 Conclusions

We performed continuous measurements of atmospheric nitrous acid (HONO) at Back Garden supersite (BG) in Pearl River Delta (PRD) in China, for 4 weeks in July 2006. The observed HONO concentrations are among the highest ever reported for rural areas, consistent with the fact that the PRD is one of the "hot-spots" of the HONO precursor NO$_2$ in the world.

Different from former studies in the same region (Su et al., 2008a,b; Qin et al., 2009), we for the first time have a full set of online measurements which are relevant for exploring the HONO formation. It is found that the direct emissions from combustion processes only have minor influence on the observed HONO concentration. During night, the reaction of OH + NO and the heterogeneous conversion of NO$_2$ on ground surfaces are the major sources of HONO. The observed net HONO production from OH + NO reaction can be up to 0.28 ppb h^{-1}. The average conversion frequency of NO$_2$ to HONO was found to be 0.024 h^{-1} which is higher than other places in the world. During daytime, to sustain the HONO concentration at ≈ 200 ppt, an additional HONO production (P_M) rate of 0.77 ppb h^{-1} is needed in addition to the productions from the well-known gas phase reactions. Our analysis demonstrated that, P_M did not relate to the heterogeneous NO$_2$ conversion, but relate to the photolysis of adsorbed HNO$_3$ on ground surfaces. There is the possibility that an unknown portion of P_M is correlated with the soil

nitrite. However, the validation of this assumption requires on-site measurements of the soil chemical and physical properties.

References

Acker, K., Möller, D., Auel, R., Wieprecht, W., and Kalass, D.: Concentrations of nitrous acid, nitric acid, nitrite and nitrate in the gas and aerosol phase at a site in the emission zone during ESCOMPTE 2001 experiment, Atmos. Res., 74, 507–524, doi:10.1016/j.atmosres.2004.04.009, 2005.

Acker, K., Febo, A., Trick, S., Perrino, C., Bruno, P., Wiesen, P., Möller, D., Wieprecht, W., Auel, R., Giusto, M., Geyer, A., Platt, U., and Allegrini, I.: Nitrous acid in the urban area of Rome, Atmos. Environ., 40, 3123–3133, doi:10.1016/j.atmosenv.2006.01.028, 2006a.

Acker, K., Möller, D., Wieprecht, W., Meixner, F. X., Bohn, B., Gilge, S., Plass-Dülmer, C., and Berresheim, H.: Strong daytime production of OH from HNO$_2$ at a rural mountain site, Geophys. Res. Lett., 33, L02809, doi:10.1029/2005gl024643, 2006b.

Akimoto, H., Takagi, H., and Sakamaki, F.: Photoenhancement of the nitrous acid formation in the surface reaction of nitrogen dioxide and water vapor: Extra radical source in smog chamber experiments, Int. J. Chem. Kinet., 19, 539–551, doi:10.1002/kin.550190606, 1987.

Alicke, B., Platt, U., and Stutz, J.: Impact of nitrous acid photolysis on the total hydroxyl radical budget during the Limitation of Oxidant Production/Pianura Padana Produzione di Ozono study in Milan, J. Geophys. Res., 107, 8196, doi:10.1029/2000jd000075, 2002.

Alicke, B., Geyer, A., Hofzumahaus, A., Holland, F., Konrad, S., Pätz, H. W., Schäfer, J., Stutz, J., Volz-Thomas, A., and Platt, U.: OH formation by HONO photolysis during the BERLIOZ experiment, J. Geophys. Res., 108, 8247, doi:10.1029/2001jd000579, 2003.

Amedro, D., Parker, A. E., Schoemaecker, C., and Fittschen, C.: Direct observation of OH radicals after 565 nm multi-photon excitation of NO$_2$ in the presence of H$_2$O, Chem. Phys. Lett., 513, 12–16, doi:10.1016/j.cplett.2011.07.062, 2011.

Ammann, M., Kalberer, M., Jost, D. T., Tobler, L., Rossler, E., Piguet, D., Gaggeler, H. W., and Baltensperger, U.: Heterogeneous production of nitrous acid on soot in polluted air masses, Nature, 395, 157–160, doi:10.1038/25965, 1998.

Ammann, M., Rossler, E., Strekowski, R., and George, C.: Nitrogen dioxide multiphase chemistry: uptake kinetics on aqueous solutions containing phenolic compounds, Phys. Chem. Chem. Phys., 7, 2513–2518, doi:10.1039/b501808k, 2005.

Aubin, D. G. and Abbatt, J. P. D.: Interaction of NO$_2$ with hydrocarbon soot: focus on HONO yield, surface modification, and mechanism, J. Phys. Chem. A, 111, 6263–6273, doi:10.1021/jp068884h, 2007.

Beine, H. J., Amoroso, A., Dominé, F., King, M. D., Nardino, M., Ianniello, A., and France, J. L.: Surprisingly small HONO emissions from snow surfaces at Browning Pass, Antarctica, Atmos. Chem. Phys., 6, 2569–2580, doi:10.5194/acp-6-2569-2006, 2006.

Bejan, I., Abd El Aal, Y., Barnes, I., Benter, T., Bohn, B., Wiesen, P., and Kleffmann, J.: The photolysis of ortho-nitrophenols: a new gas phase source of HONO, Phys. Chem. Chem. Phys., 8, 2028–2035, doi:10.1039/B516590C, 2006.

Bohn, B., Corlett, G. K., Gillmann, M., Sanghavi, S., Stange, G., Tensing, E., Vrekoussis, M., Bloss, W. J., Clapp, L. J., Kortner, M., Dorn, H.-P., Monks, P. S., Platt, U., Plass-Dülmer, C., Mihalopoulos, N., Heard, D. E., Clemitshaw, K. C., Meixner, F. X., Prevot, A. S. H., and Schmitt, R.: Photolysis frequency measurement techniques: results of a comparison within the ACCENT project, Atmos. Chem. Phys., 8, 5373–5391, doi:10.5194/acp-8-5373-2008, 2008.

Bröske, R., Kleffmann, J., and Wiesen, P.: Heterogeneous conversion of NO_2 on secondary organic aerosol surfaces: A possible source of nitrous acid (HONO) in the atmosphere?, Atmos. Chem. Phys., 3, 469–474, doi:10.5194/acp-3-469-2003, 2003.

Carr, S., Heard, D. E., and Blitz, M. A.: Comment on "Atmospheric hydroxyl radical production from electronically excited NO_2 and H_2O", Science, 324, 336–336, doi:10.1126/science.1166669, 2009.

Chan, C. K. and Yao, X.: Air pollution in mega cities in China, Atmos. Environ., 42, 1–42, doi:10.1016/j.atmosenv.2007.09.003, 2008.

Cheng, M.-T., Horng, C.-L., and Lin, Y.-C.: Characteristics of atmospheric aerosol and acidic gases from urban and forest sites in Central Taiwan, B. Environ. Contam. Tox., 79, 674–677, doi:10.1007/s00128-007-9296-2, 2007.

Cheng, M.-T., Chen, S.-P., Lin, Y.-C., Jung, C.-C., and Horng, C.-L.: Concentrations and formation rates of ambient nitrous acid in Taichung City, Taiwan, Environ. Eng. Sci., 25, 1149–1158, doi:10.1089/ees.2007.0124, 2008.

Dusanter, S., Vimal, D., Stevens, P. S., Volkamer, R., and Molina, L. T.: Measurements of OH and HO_2 concentrations during the MCMA-2006 field campaign – Part 1: Deployment of the Indiana University laser-induced fluorescence instrument, Atmos. Chem. Phys., 9, 1665–1685, doi:10.5194/acp-9-1665-2009, 2009.

Elshorbany, Y. F., Kurtenbach, R., Wiesen, P., Lissi, E., Rubio, M., Villena, G., Gramsch, E., Rickard, A. R., Pilling, M. J., and Kleffmann, J.: Oxidation capacity of the city air of Santiago, Chile, Atmos. Chem. Phys., 9, 2257–2273, doi:10.5194/acp-9-2257-2009, 2009.

Febo, A., Perrino, C., and Allegrini, I.: Measurement of nitrous acid in milan, italy, by doas and diffusion denuders, Atmos. Environ., 30, 3599–3609, doi:10.1016/1352-2310(96)00069-6, 1996.

Finlayson-Pitts, B. J. and Pitts, J. N.: Chemistry of the Upper and Lower Atmosphere – Theory, Experiments and Applications, 1st edn., Academic Press, San Diego, USA, 2000.

Finlayson-Pitts, B. J., Wingen, L. M., Sumner, A. L., Syomin, D., and Ramazan, K. A.: The heterogeneous hydrolysis of NO_2 in laboratory systems and in outdoor and indoor atmospheres: an integrated mechanism, Phys. Chem. Chem. Phys., 5, 223–242, doi:10.1039/B208564J, 2003.

Garland, R. M., Yang, H., Schmid, O., Rose, D., Nowak, A.,

Achtert, P., Wiedensohler, A., Takegawa, N., Kita, K., Miyazaki, Y., Kondo, Y., Hu, M., Shao, M., Zeng, L. M., Zhang, Y. H., Andreae, M. O., and Pöschl, U.: Aerosol optical properties in a rural environment near the mega-city Guangzhou, China: implications for regional air pollution, radiative forcing and remote sensing, Atmos. Chem. Phys., 8, 5161–5186, doi:10.5194/acp-8-5161-2008, 2008.

George, C., Strekowski, R. S., Kleffmann, J., Stemmler, K., and Ammann, M.: Photoenhanced uptake of gaseous NO_2 on solid organic compounds: a photochemical source of HONO?, Faraday Discuss., 130, 195–210, doi:10.1039/B417888M, 2005.

Hao, N., Zhou, B., Chen, D., and Chen, L.: Observations of nitrous acid and its relative humidity dependence in Shanghai, J. Environ. Sci., 18, 910–915, doi:10.1016/S1001-0742(06)60013-2, 2006.

Harrison, R. M. and Kitto, A.-M. N.: Evidence for a surface source of atmospheric nitrous acid, Atmos. Environ., 28, 1089–1094, doi:10.1016/1352-2310(94)90286-0, 1994.

Harrison, R. M., Peak, J. D., and Collins, G. M.: Tropospheric cycle of nitrous acid, J. Geophys. Res., 101, 14429–14439, doi:10.1029/96jd00341, 1996.

Heland, J., Kleffmann, J., Kurtenbach, R., and Wiesen, P.: A new instrument to measure gaseous nitrous acid (HONO) in the atmosphere, Environ. Sci. Technol., 35, 3207–3212, doi:10.1021/es000303t, 2001.

Hofzumahaus, A., Rohrer, F., Lu, K., Bohn, B., Brauers, T., Chang, C.-C., Fuchs, H., Holland, F., Kita, K., Kondo, Y., Li, X., Lou, S., Shao, M., Zeng, L., Wahner, A., and Zhang, Y.: Amplified trace gas removal in the Troposphere, Science, 324, 1702–1704, doi:10.1126/science.1164566, 2009.

Kanaya, Y., Cao, R., Akimoto, H., Fukuda, M., Komazaki, Y., Yokouchi, Y., Koike, M., Tanimoto, H., Takegawa, N., and Kondo, Y.: Urban photochemistry in central Tokyo: 1. Observed and modeled OH and HO_2 radical concentrations during the winter and summer of 2004, J. Geophys. Res., 112, D21312, doi:10.1029/2007jd008670, 2007.

Kleffmann, J., Becker, K. H., and Wiesen, P.: Heterogeneous NO_2 conversion processes on acid surfaces: possible atmospheric implications, Atmos. Environ., 32, 2721–2729, doi:10.1016/s1352-2310(98)00065-x, 1998.

Kleffmann, J., Becker, K. H., Lackhoff, M., and Wiesen, P.: Heterogeneous conversion of NO_2 on carbonaceous surfaces, Phys. Chem. Chem. Phys., 1, 5443–5450, doi:10.1039/A905545B, 1999.

Kleffmann, J., Gavriloaiei, T., Hofzumahaus, A., Holland, F., Koppmann, R., Rupp, L., Schlosser, E., Siese, M., and Wahner, A.: Daytime formation of nitrous acid: a major source of OH radicals in a forest, Geophys. Res. Lett., 32, L05818, doi:10.1029/2005gl022524, 2005.

Kleffmann, J., Lörzer, J. C., Wiesen, P., Kern, C., Trick, S., Volkamer, R., Rodenas, M., and Wirtz, K.: Intercomparison of the DOAS and LOPAP techniques for the detection of nitrous acid (HONO), Atmos. Environ., 40, 3640–3652, doi:10.1016/j.atmosenv.2006.03.027, 2006.

Kurtenbach, R., Becker, K. H., Gomes, J. A. G., Kleffmann, J., Lörzer, J. C., Spittler, M., Wiesen, P., Ackermann, R., Geyer, A., and Platt, U.: Investigations of emissions and heterogeneous formation of HONO in a road traffic tunnel, Atmos. Environ., 35, 3385–3394, doi:10.1016/s1352-2310(01)00138-8, 2001.

Lammel, G.: Formation of Nitrous acid: Parameterisation and comparison with observatins, Technical report, Max-Planck Institute for Meteorology, Hamburg, Germany, 1999.

Lammel, G. and Cape, J. N.: Nitrous acid and nitrite in the atmosphere, Chem. Soc. Rev., 25, 361–369, doi:10.1039/CS9962500361, 1996.

Li, S., Matthews, J., and Sinha, A.: Atmospheric hydroxyl radical production from electronically excited NO_2 and H_2O, Science, 319, 1657–1660, doi:10.1126/science.1151443, 2008.

Li, X., Brauers, T., Shao, M., Garland, R. M., Wagner, T., Deutschmann, T., and Wahner, A.: MAX-DOAS measurements in Southern China: retrieval of aerosol extinctions and validation using ground-based in-situ data, Atmos. Chem. Phys., 10, 2079-2089, doi:10.5194/acp-10-2079-2010, 2010.

Liu, X., Cheng, Y., Zhang, Y., Jung, J., Sugimoto, N., Chang, S.-Y., Kim, Y. J., Fan, S., and Zeng, L.: Influences of relative humidity and particle chemical composition on aerosol scattering properties during the 2006 PRD campaign, Atmos. Environ., 42, 1525–1536, doi:10.1016/j.atmosenv.2007.10.077, 2008.

Lou, S., Holland, F., Rohrer, F., Lu, K., Bohn, B., Brauers, T., Chang, C. C., Fuchs, H., Häseler, R., Kita, K., Kondo, Y., Li, X., Shao, M., Zeng, L., Wahner, A., Zhang, Y., Wang, W., and Hofzumahaus, A.: Atmospheric OH reactivities in the Pearl River Delta – China in summer 2006: measurement and model results, Atmos. Chem. Phys., 10, 11243–11260, doi:10.5194/acp-10-11243-2010, 2010.

Lu, K. D., Rohrer, F., Holland, F., Fuchs, H., Bohn, B., Brauers, T., Chang, C. C., Hseler, R., Hu, M., Kita, K., Kondo, Y., Li, X., Lou, S. R., Nehr, S., Shao, M., Zeng, L. M., Wahner, A., Zhang, Y. H., and Hofzumahaus, A.: Observation and modelling of OH and HO_2 concentrations in the Pearl River Delta 2006: a missing OH source in a VOC rich atmosphere, Atmos. Chem. Phys. Discuss., 11, 11311–11378, doi:10.5194/acpd-11-11311-2011, 2011.

Qin, M., Xie, P., Su, H., Gu, J., Peng, F., Li, S., Zeng, L., Liu, J., Liu, W., and Zhang, Y.: An observational study of the HONO-NO_2 coupling at an urban site in Guangzhou City, South China, Atmos. Environ., 43, 5731–5742, doi:10.1016/j.atmosenv.2009.08.017, 2009.

Ren, X., Gao, H., Zhou, X., Crounse, J. D., Wennberg, P. O., Browne, E. C., LaFranchi, B. W., Cohen, R. C., McKay, M., Goldstein, A. H., and Mao, J.: Measurement of atmospheric nitrous acid at Bodgett Forest during BEARPEX2007, Atmos. Chem. Phys., 10, 6283–6294, doi:10.5194/acp-10-6283-2010, 2010.

Richter, A., Burrows, J. P., Nusz, H., Granier, C., and Niemeier, U.: Increase in tropospheric nitrogen dioxide over China observed from space, Nature, 437, 129–132, doi:10.1038/nature04092, 2005.

Rohrer, F., Bohn, B., Brauers, T., Brüning, D., Johnen, F.-J., Wahner, A., and Kleffmann, J.: Characterisation of the photolytic HONO-source in the atmosphere simulation chamber SAPHIR, Atmos. Chem. Phys., 5, 2189–2201, doi:10.5194/acp-5-2189-2005, 2005.

Shon, Z. H., Lee, G., Song, S. K., Lee, M., Han, J., and Lee, D.: Characteristics of reactive nitrogen compounds and other relevant trace gases in the atmosphere at urban and rural areas of Korea during May–June, 2004, J. Atmos. Chem., 58, 203–218, doi:10.1007/s10874-007-9088-4, 2007.

Song, C. H., Park, M. E., Lee, E. J., Lee, J. H., Lee, B. K., Lee, D. S., Kim, J., Han, J. S., Moon, K. J., and Kondo, Y.: Possible particulate nitrite formation and its atmospheric implications inferred from the observations in Seoul, Korea, Atmos. Environ., 43, 2168–2173, doi:10.1016/j.atmosenv.2009.01.018, 2009.

Sörgel, M., Regelin, E., Bozem, H., Diesch, J.-M., Drewnick, F., Fischer, H., Harder, H., Held, A., Hosaynali-Beygi, Z., Martinez, M., and Zetzsch, C.: Quantification of the unknown HONO daytime source and its relation to NO_2, Atmos. Chem. Phys., 11, 10433–10447, doi:10.5194/acp-11-10433-2011, 2011a.

Sörgel, M., Trebs, I., Serafimovich, A., Moravek, A., Held, A., and Zetzsch, C.: Simultaneous HONO measurements in and above a forest canopy: influence of turbulent exchange on mixing ratio differences, Atmos. Chem. Phys., 11, 841–855, doi:10.5194/acp-11-841-2011, 2011b.

Spindler, G., Brüggemann, E., and Herrmann, H.: Nitrous acid concentration measurements and estimation of dry deposition over grassland in Eastern Germany, in: Proceedings of the EUROTRAC Symposium 1998, Vol. 2, WITpress, Southampton, UK, 218–222, 1999.

Stemmler, K., Ammann, M., Donders, C., Kleffmann, J., and George, C.: Photosensitized reduction of nitrogen dioxide on humic acid as a source of nitrous acid, Nature, 440, 195–198, doi:10.1038/nature04603, 2006.

Stemmler, K., Ndour, M., Elshorbany, Y., Kleffmann, J., D'Anna, B., George, C., Bohn, B., and Ammann, M.: Light induced conversion of nitrogen dioxide into nitrous acid on submicron humic acid aerosol, Atmos. Chem. Phys., 7, 4237–4248, doi:10.5194/acp-7-4237-2007, 2007.

Stutz, J., Alicke, B., and Neftel, A.: Nitrous acid formation in the urban atmosphere: gradient measurements of NO_2 and HONO over grass in Milan, Italy, J. Geophys. Res., 107, 8192, doi:10.1029/2001jd000390, 2002.

Stutz, J., Alicke, B., Ackermann, R., Geyer, A., Wang, S., White, A. B., Williams, E. J., Spicer, C. W., and Fast, J. D.: Relative humidity dependence of HONO chemistry in urban areas, J. Geophys. Res., 109, D03307, doi:10.1029/2003jd004135, 2004.

Su, H., Cheng, Y. F., Cheng, P., Zhang, Y. H., Dong, S., Zeng, L. M., Wang, X., Slanina, J., Shao, M., and Wiedensohler, A.: Observation of nighttime nitrous acid (HONO) formation at a non-urban site during PRIDE-PRD2004 in China, Atmos. Environ., 42, 6219–6232, doi:10.1016/j.atmosenv.2008.04.006, 2008a.

Su, H., Cheng, Y. F., Shao, M., Gao, D. F., Yu, Z. Y., Zeng, L. M., Slanina, J., Zhang, Y. H., and Wiedensohler, A.: Nitrous acid (HONO) and its daytime sources at a rural site during the 2004 PRIDE-PRD experiment in China, J. Geophys. Res., 113, D14312, doi:10.1029/2007jd009060, 2008b.

Su, H., Cheng, Y., Oswald, R., Behrendt, T., Trebs, I., Meixner, F. X., Andreae, M. O., Cheng, P., Zhang, Y., and Pöschl, U.: Soil Nitrite as a Source of Atmospheric HONO and OH Radicals, Science, 333, 1616–1618, doi:10.1126/science.1207687, 2011.

Takegawa, N., Miyakawa, T., Kondo, Y., Jimenez, J. L., Zhang, Q., Worsnop, D. R., and Fukuda, M.: Seasonal and diurnal variations of submicron organic aerosol in Tokyo observed using the Aerodyne aerosol mass spectrometer, J. Geophys. Res., 111, D11206, doi:10.1029/2005jd006515, 2006.

Trick, S.: Formation of nitrous acid on urban surfaces, Ph.D. thesis, Universität Heidelberg, Heidelberg, Germany, 2004.

Wong, K. W., Oh, H.-J., Lefer, B. L., Rappenglück, B., and Stutz, J.: Vertical profiles of nitrous acid in the nocturnal urban atmosphere of Houston, TX, Atmos. Chem. Phys., 11, 3595–3609, doi:10.5194/acp-11-3595-2011, 2011.

Wong, K. W., Tsai, C., Lefer, B., Haman, C., Grossberg, N., Brune, W. H., Ren, X., Luke, W., and Stutz, J.: Daytime HONO Vertical gradients during SHARP 2009 in Houston, TX, Atmos. Chem. Phys., 12, 635–652, doi:10.5194/acp-12-635-2012, 2012.

Yang, Q., Su, H., Brauers, T., Cheng, Y. F., Gu, J., Häseler, R., Hofzumahaus, A., Hu, M., Li, X., Lu, K., Wiedensohler, A., Zeng, L., Zhu, T., Wahner, A., and Zhang, Y.: Daytime Nitrous Acid (HONO) Formation in the Megacity Beijing, Atmos. Chem. Phys. Discuss., in preparation, 2010.

Yu, Y., Galle, B., Panday, A., Hodson, E., Prinn, R., and Wang, S.: Observations of high rates of NO_2-HONO conversion in the nocturnal atmospheric boundary layer in Kathmandu, Nepal, Atmos. Chem. Phys., 9, 6401–6415, doi:10.5194/acp-9-6401-2009, 2009.

Yue, D. L., Hu, M., Wu, Z. J., Guo, S., Wen, M. T., Nowak, A., Wehner, B., Wiedensohler, A., Takegawa, N., Kondo, Y., Wang, X. S., Li, Y. P., Zeng, L. M., and Zhang, Y. H.: Variation of particle number size distributions and chemical compositions at the urban and downwind regional sites in the Pearl River Delta during summertime pollution episodes, Atmos. Chem. Phys., 10, 9431–9439, doi:10.5194/acp-10-9431-2010, 2010.

Zhang, B. and Tao, F.-M.: Direct homogeneous nucleation of NO_2, H_2O, and NH_3 for the production of ammonium nitrate particles and HONO gas, Chem. Phys. Lett., 489, 143–147, doi:10.1016/j.cplett.2010.02.059, 2010.

Zhang, Y. H., Hu, M., M., S., Brauers, T., Chang, C. C., Hofzumahaus, A., Holland, F., Li, X., Lu, K., Kondo, Y., Nowak, A., Pöschl, U., Rohrer, F., Zeng, L., Wiedensohler, A., and Wahner, A.: Continuous efforts to investigate regional air pollution in the Pearl River Delta, China: PRIDE-PRD2006 campaign, Atmos. Chem. Phys., in preparation, 2012.

Zhou, X., He, Y., Huang, G., Thornberry, T. D., Carroll, M. A., and Bertman, S. B.: Photochemical production of nitrous acid on glass sample manifold surface, Geophys. Res. Lett., 29, 1681, doi:10.1029/2002gl015080, 2002.

Zhou, X., Gao, H., He, Y., Huang, G., Bertman, S. B., Civerolo, K., and Schwab, J.: Nitric acid photolysis on surfaces in low-NO_x environments: significant atmospheric implications, Geophys. Res. Lett., 30, 2217, doi:10.1029/2003gl018620, 2003.

Zhou, X., Huang, G., Civerolo, K., Roychowdhury, U., and Demerjian, K. L.: Summertime observations of HONO, HCHO, and O_3 at the summit of Whiteface Mountain, New York, J. Geophys. Res., 112, D08 311, doi:10.1029/2006jd007256, 2007.

Zhou, X. et al.: Nitric acid photolysis on forest canopy surface as a source for tropospheric nitrous acid, Nature Geosci, 4, 440–443, doi:10.1038/ngeo1164, 2011.